Analysis of characteristics of bent rib waveguides

Daoxin Dai

Centre for Optical and Electromagnetic Research, Joint Laboratory of Optical Communications of Zhejiang University, State Key Laboratory for Modern Optical Instrumentation, Zhejiang University, Yu-Quan, Hangzhou 310027, China

Sailing He

Centre for Optical and Electromagnetic Research, Joint Laboratory of Optical Communications of Zhejiang University, State Key Laboratory for Modern Optical Instrumentation, Zhejiang University, Yu-Quan, Hangzhou 310027, China, and Division of Electromagnetic Theory, Alfven Laboratory, Royal Institute of Technology, S-100 44 Stockholm, Sweden

Received April 24, 2003; revised manuscript received August 11, 2003; accepted September 2, 2003

With a perfectly matched layer boundary treatment, a semivectorial finite-difference method is used to calculate the eigenmodes of a single-mode (SM) or multimode (MM) bent rib waveguide. A detailed analysis is given for the dependence of the bending losses (including the pure bending loss and the transition loss) on geometrical parameters of the bent rib waveguide such as the rib width, the rib height, and the bending radius. The characteristics of the higher-order modes are analyzed. It is shown that the bending loss of the fundamental mode can be reduced effectively by increasing the width and height of the rib. For an integrated device, undesired effects due to the higher-order modes of a MM bent waveguide can be removed by appropriate choice of the geometrical parameters. An appropriately designed MM bent waveguide is used to reduce effectively the bending loss of the fundamental mode, and a low-loss SM propagation in a MM bent waveguide is realized when the bending losses of the higher-order modes are large enough. © 2004 Optical Society of America

OCIS codes: 130.2790, 230.7370, 230.7380.

1. INTRODUCTION

It is well known that a bent waveguide is an essential element for photonic integrated circuits (PICs). The characteristics of bent waveguides have been given much attention, especially the characteristics of bending losses (including the pure bending loss and the transition loss).[1,2] Usually, the bending loss increases when the bending radius decreases. Thus one has to increase the bending radius to reduce the bending loss. However, the total size of the PIC will then become large, which is not good for achieving a high integration density.

Rib waveguides are very popular for PICs. When the height of the rib increases, the rib waveguide may become strongly confined, which can reduce the bending loss greatly. The bending loss can also be reduced by increase in the width of the rib. It is well known that a channel waveguide is usually required to be single mode (SM) in many PICs such as arrayed waveguide gratings (AWGs).[3] Therefore the height or width of the rib should be chosen to satisfy the corresponding SM condition. Previous analyses for bent wave guides are mainly for the fundamental mode of a SM bent waveguide.

In the present paper a detailed analysis for a multimode (MM) bent waveguide is given. As we know, the bending loss of a higher-order mode is usually much larger than that of the fundamental mode. By appropriate choice of the geometrical parameters of the bent waveguide, the power of the higher-order modes can attenuate rapidly along the propagation direction, and thus bad effects due to the higher-order modes can be reduced. At the same time, the bending loss of the fundamental mode can be kept low. In this way, only one mode (the fundamental mode) can propagate with a low loss in a MM bent waveguide. When the height or width of the rib increases (and the waveguide becomes MM), the bending loss for the fundamental mode of a bent waveguide is reduced. Thus an appropriately designed MM bent waveguide can be used to reduce effectively the bending loss of the fundamental mode.

By use of a finite-difference method (FDM) with a perfectly matched layer boundary treatment, the eigenmodes of a bent rib waveguide are calculated accurately in the present paper. The real part of the propagation constant represents the phase variation along the propagation direction, and the imaginary part represents the pure bending loss. The transition loss can be calculated from an overlapped integral of the eigenmode fields of the two waveguides connected to each other.

2. THEORY

A. Semivectorial Finite-Difference Method

For a bent waveguide, the Dirichlet condition is not appropriate for use as the boundary condition, and a perfectly matched layer boundary treatment is preferred in a FDM. In a complex coordinate system (the cross section of the waveguide is in the xy plane), the full-vector wave equation for the electric field is given by[4]

$$\begin{bmatrix} P_{xx} & P_{xy} \\ P_{yx} & P_{yy} \end{bmatrix} \begin{pmatrix} E_x \\ E_y \end{pmatrix} = \frac{1}{\tilde{t}_x^{\,2}} \frac{\partial^2}{\partial z^2} \begin{pmatrix} E_x \\ E_y \end{pmatrix}, \tag{1}$$

where

$$P_{xx}E_x = \frac{1}{\tilde{t}_x{}^2}\frac{\partial}{\partial\tilde{x}}\left[\frac{\tilde{t}_x}{n^2}\frac{\partial(\tilde{t}_x n^2 E_x)}{\partial\tilde{x}}\right] + \frac{\partial^2 E_x}{\partial\tilde{y}^2} + n^2 k_0{}^2 E_x,$$

$$P_{xy}E_y = \frac{1}{\tilde{t}_x{}^2}\frac{\partial}{\partial\tilde{x}}\left[\frac{\tilde{t}_x{}^2}{n^2}\frac{\partial(n^2 E_y)}{\partial\tilde{y}}\right] - \frac{\partial^2 E_y}{\partial\tilde{x}\partial\tilde{y}},$$

$$P_{yy}E_y = \frac{\partial}{\partial\tilde{y}}\left[\frac{1}{n^2}\frac{\partial(n^2 E_y)}{\partial\tilde{y}}\right] + \frac{1}{\tilde{t}_x}\frac{\partial}{\partial\tilde{x}}\left(\tilde{t}_x\frac{\partial E_y}{\partial\tilde{x}}\right) + n^2 k_0{}^2 E_y,$$

$$P_{yx}E_x = \frac{\partial}{\partial\tilde{y}}\left[\frac{1}{\tilde{t}_x n^2}\frac{\partial(\tilde{t}_x n^2 E_x)}{\partial\tilde{x}}\right] - \frac{1}{\tilde{t}_x}\frac{\partial}{\partial\tilde{x}}\left(\tilde{t}_x\frac{\partial E_x}{\partial\tilde{y}}\right),$$

and where n is the refractive-index profile, k_0 is the wave number in vacuum, and $\tilde{t}_x = 1 + \tilde{x}/R$, ($R$ is the bending radius). Let $E_x = \bar{E}_x \exp(-j\beta z)$ and $E_y = \bar{E}_y \exp(-j\beta z)$. Substituting them into Eq. (1), one obtains the following semivectorial eigenequations for quasi-TE and quasi-TM modes [with the coupling terms P_{xy} and P_{yx} in Eq. (1) neglected]:

$$P_{xx}\bar{E}_x = \frac{1}{\tilde{t}_x{}^2}\beta^2\bar{E}_x, \tag{2a}$$

$$P_{yy}\bar{E}_y = \frac{1}{\tilde{t}_x{}^2}\beta^2\bar{E}_y. \tag{2b}$$

Using a central-grid finite-difference formula for Eq. (2a), one obtains the following eigenequation for quasi-TE modes:

$$a_{mn}\cdot\bar{E}_x(m-1,n) + b_{mn}\cdot\bar{E}_x(m,n) + c_{mn}\cdot\bar{E}_x(m+1,n) + d_{mn}\bar{E}_x(m,n-1) + e_{mn}\bar{E}_x(m,n+1) = \beta^2\cdot\bar{E}_x(m,n), \tag{3}$$

where

$$a_{mn} = \frac{n_{m-1}{}^2(1+\tilde{x}_{m-1}/R)}{2\Delta\tilde{x}_m\Delta\tilde{x}_{m-1/2}}\times\left(\frac{1+\tilde{x}_{m-1}/R}{n_{m-1}{}^2} + \frac{1+\tilde{x}_m/R}{n_m{}^2}\right),$$

$$b_{mn} = -\frac{(1+\tilde{x}_m/R)n_m{}^2}{2\Delta\tilde{x}_m}\times\left[\left(\frac{1+\tilde{x}_{m+1}/R}{n_{m+1}{}^2} + \frac{1+\tilde{x}_m/R}{n_m{}^2}\right)\frac{1}{\Delta\tilde{x}_{m+1/2}} + \left(\frac{1+\tilde{x}_{m-1}/R}{n_{m-1}{}^2} + \frac{1+\tilde{x}_m/R}{n_m{}^2}\right)\frac{1}{\Delta\tilde{x}_{m-1/2}}\right] - \frac{(1+\tilde{x}_m/R)^2}{\Delta\tilde{y}_n}\left(\frac{1}{\Delta\tilde{y}_{n+1/2}} + \frac{1}{\Delta\tilde{y}_{n-1/2}}\right) + n_{mn}{}^2 k_0{}^2(1+\tilde{x}_m/R)^2,$$

$$c_{mn} = \frac{n_{m+1}{}^2(1+\tilde{x}_{m+1}/R)}{2\Delta\tilde{x}_m\Delta\tilde{x}_{m+1/2}}\times\left(\frac{1+\tilde{x}_{m+1}/R}{n_{m+1}{}^2} + \frac{1+\tilde{x}_m/R}{n_m{}^2}\right),$$

$$d_{mn} = \frac{(1+\tilde{x}_m/R)^2}{\Delta\tilde{y}_n\Delta\tilde{y}_{n-1/2}},$$

$$e_{mn} = \frac{(1+\tilde{x}_m/R)^2}{\Delta\tilde{y}_n\Delta\tilde{y}_{n+1/2}},$$

and where $\Delta\tilde{x}_{m+1/2} = \tilde{x}_{m+1} - \tilde{x}_m$, $\Delta\tilde{x}_{m-1/2} = \tilde{x}_m - \tilde{x}_{m-1}$, and $\Delta\tilde{x}_m = \tilde{x}_{m+1/2} - \tilde{x}_{m-1/2}$. In a similar way, the corresponding eigenequation for quasi-TM modes can be obtained from Eq. (2b). By solving these eigenequations, one can obtain the eigenvectors (i.e., the modal field distributions) and the corresponding eigenvalues (i.e., the propagation constants for the eigenmodes). The real and imaginary parts of the propagation constant represent the phase variation and the pure bending loss, respectively.

B. Bending Losses

For a $\pi/2$ bent waveguide with a bending radius R, the pure bending loss is given by

$$L_\alpha = 20\log[\exp(\pi/2\times\beta_i R)] \quad [\text{decibels (dB)}/90^\circ]. \tag{4}$$

For a bent waveguide, the peak of the modal field distribution shifts outward and deviates from the center of the waveguide in the lateral direction. The deviation increases as the bending radius decreases. When two bent waveguides with different bending radii are connected to each other, a transition loss occurs owing to the mismatch of the modal fields. The transition loss can be calculated with the overlapped integral method. The transition loss at the junction between a straight waveguide and a bent waveguide can be calculated by

$$L_T = -10\log\left[\frac{\left|\int_{-\infty}^{+\infty}\int_{-\infty}^{+\infty} E_0(x, y)E_0{}^{B*}(x, y)\mathrm{d}x\mathrm{d}y\right|^2}{\left|\int_{-\infty}^{+\infty}\int_{-\infty}^{+\infty} E_0(x, y)E_0{}^{*}(x, y)\mathrm{d}x\mathrm{d}y\right|\left|\int_{-\infty}^{+\infty}\int_{-\infty}^{+\infty} E_0{}^{B}(x, y)E_0{}^{B*}(x, y)\mathrm{d}x\mathrm{d}y\right|}\right] \quad (\mathrm{dB}), \quad (5)$$

where * denotes complex conjugation and $E_0(x, y)$ and $E_0{}^B(x, y)$ are the modal fields for the straight waveguide and the bent waveguide, respectively.

3. RESULTS AND DISCUSSIONS

To confirm that the FDM code used in this paper is correct, we first calculate the pure bending loss for an example (shown in the inset of Fig. 1) considered earlier in the literature[5,6] and give the comparison results in Fig. 1. The solid curve, the dotted–dashed curve, and the dashed curve show the pure bending loss calculated by the present FDM, the finite-element method[5] (FEM), and the method of lines[6] (MOL), respectively. From Fig. 1, one can see that the results obtained with our FDM code agree well with earlier results in the literature.

In the rest of the paper, we choose a SOI (silicon-on-insulator) rib waveguide to analyze. The SM condition for a SOI rib waveguide is given by[7]

$$t < r/\sqrt{1 - r^2}, \quad (6)$$

where $t \approx w_r/h_2$, $r \approx (h_2 - h_r)/h_2$, w_r and h_r are the width and height of the rib, respectively, and h_2 is the total thickness of the silicon layer (see Fig. 2). The SM region and the MM region are shown in Fig. 2. The refractive indices for the core and the cladding are $n_1 = 1.0$, $n_2 = 3.455$, and $n_3 = 1.46$ (see Fig. 2).

A. Bending Losses

In this subsection we first study the dependence of the bending losses (including the pure bending loss and the transition loss) on the width of the rib. The height h_r of the rib is fixed at 2.0 μm. Figures 3(a) and 3(b) show the pure bending loss and the transition loss, respectively, of the fundamental mode $E_{11}{}^x$ as the bending radius varies. In Figs. 3(a) and 3(b) the double-dotted–dashed curves, the dashed curves, the solid curves, and the dotted–dashed curves are for the cases of $w_r = 4$, 5, 6, and 8 μm, respectively. From these figures, one sees that the bending loss decreases when the bending radius increases.

Figure 3(a) indicates that the pure bending loss decreases as the width of the rib increases for a fixed bending radius. For example, in the case of $R = 10{,}000$ μm, the pure bending loss is reduced from -12.670 to -0.078 dB when the rib width w_r increases from 4 to 8 μm. On the other hand, for an allowable pure bending loss of 0.1 dB/90°, the minimal radii are approximately 24,000, 15,000, 11,800, and 9800 μm for the cases of $w_r = 4$, 5, 6, and 8 μm, respectively. Thus the bending radius can be greatly reduced by increase in the rib width. This is good for minimizing the device size and increasing the integration density.

Note that the pure bending loss cannot be reduced much further when the rib width reaches a certain value. For example, when $R = 10{,}000$ μm the pure bending loss is reduced by 10.893 dB as the rib width increases from 4 to 5 μm [see Fig. 3(a)]. However, the reduction in the pure bending loss is only 0.318 dB when the rib width increases from 6 to 8 μm.

From Fig. 3(b) one sees that the transition loss decreases to a minimal value and then starts to increase as the rib width increases for a fixed bending radius. This is different from the monotonous characteristic of the pure bending loss shown in Fig. 3(a). The transition loss as the rib width increases for different bending radii is shown in Fig. 4, from which one can see that there exists an optimal value of the rib width for a minimal transition loss. The optimal width is not sensitive to the bending

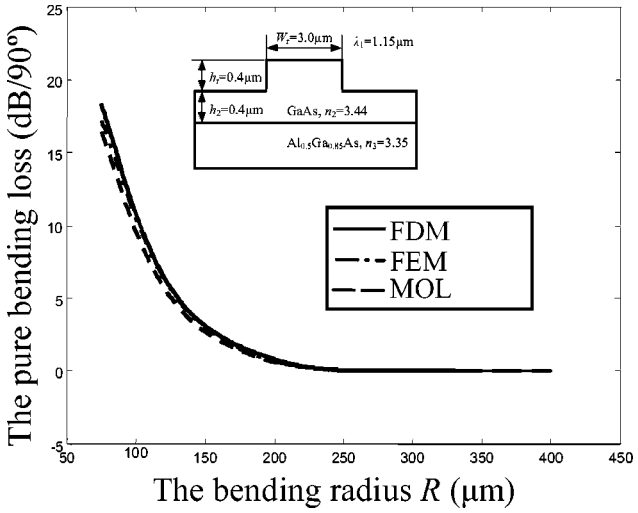

Fig. 1. Comparison of the pure bending loss calculated with the present FDM code, FEM,[5] and MOL[6] for an example (shown in the inset) considered in Ref. 5.

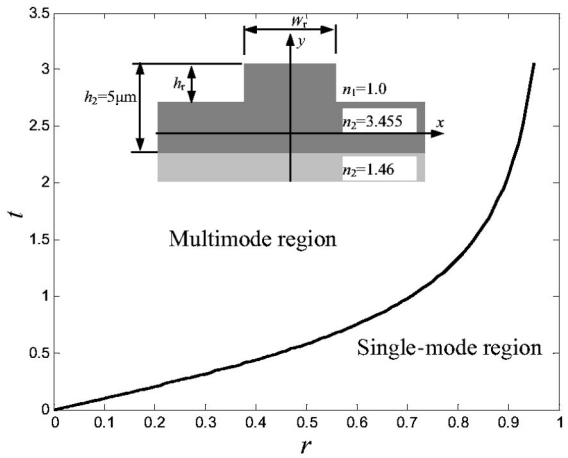

Fig. 2. SM region and the MM region for a SOI rib waveguide.

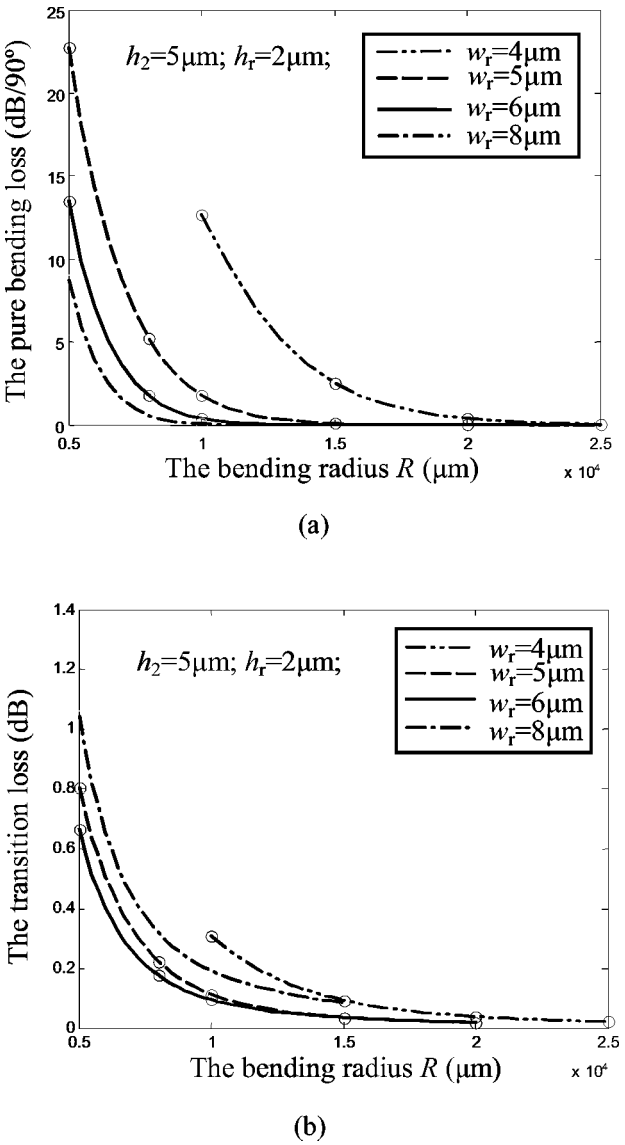

Fig. 3. Bending loss as the bending radius varies for SOI rib waveguides with different rib widths. (a) The pure bending loss. (b) The transition bending loss.

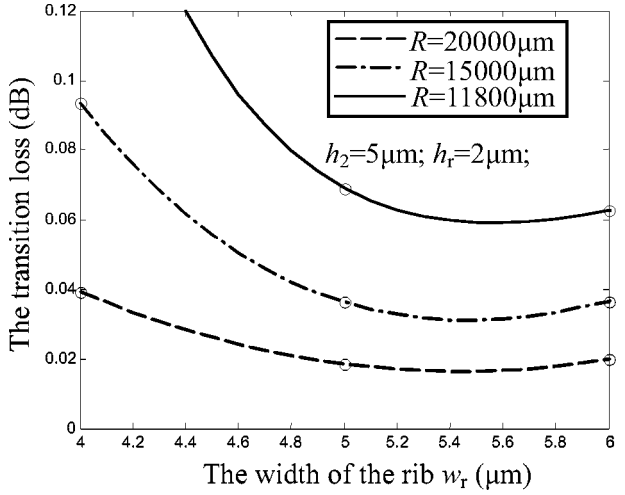

Fig. 4. Transition loss as the rib width increases for different bending radii (here h_r = 2 μm).

radius. Thus we choose a fixed bending radius to show how the transition loss varies as the rib width increases for different rib heights in Fig. 5. Here the bending radii are chosen in such a way that the pure bending loss is lower than 0.1 dB/90°. From Fig. 3(a) one sees that the corresponding bending radii are 11,800, 4550, and 1800 μm for the cases of h_r = 2, 2.5, and 3 μm, respectively.

From Fig. 5 one can see that the optimal value of the rib width increases when the rib height decreases. This can be explained by analysis of the field distribution of the fundamental mode. Figures 6(a)–6(c) show the fundamental modal fields for the cases of w_r = 4, 6, and 8 μm, respectively, when R = 10,000 μm and h_r = 2 μm. From these figures one can see that when the rib width increases the power leaking outward decreases, which results in a reduction of the transition loss. However, at the same time the peak deviation of the field distribution from the central axis of the waveguide increases (see Fig. 5), which increases the transition loss. Figure 6 shows that the peak deviations are approximately 0.25, 0.4, and 0.9 μm when w_r = 4, 6, and 8 μm, respectively. Both factors affect the transition loss and result in a nonmonotonous variation of the transition loss as shown in Fig. 5. The above transition loss is calculated when the central axis of the straight waveguide coincides with that of the bent waveguide. For a weakly confined waveguide, one can reduce further the transition loss by introducing a lateral offset between the central axes of the straight waveguide and the bent waveguide.[8] However, for a SOI rib waveguide, such a lateral offset will cause a facet reflection, since the refractive-index difference between Si and air is very large.

Compared with the increase of the rib width, the increase of the rib height can reduce the bending loss more effectively. According to the SM condition given by inequality (6), higher-order modes will appear when the rib width or height increases. The higher-order modes will introduce some undesired effects for an integrated waveguide device, for example, the cross talk between adjacent channels in an AWG.

Here we analyze the higher-order modes for the case of h_r = 3 μm. Figures 7(a)–7(f) show the pure bending

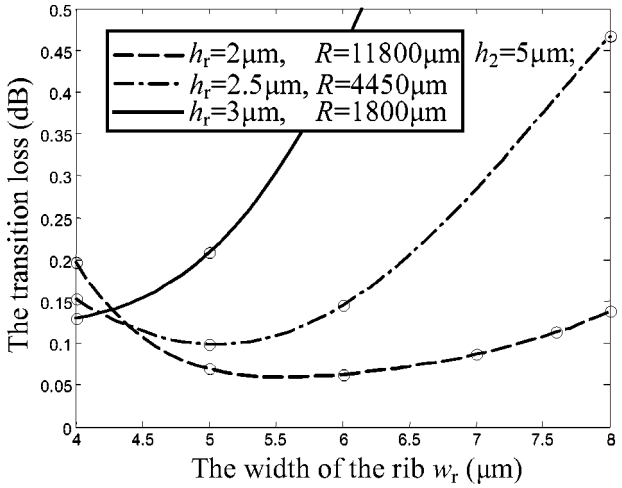

Fig. 5. Transition loss as the rib width increases for different rib depths and bending radii.

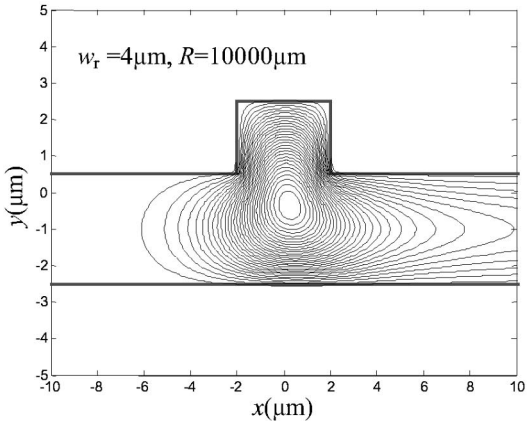

(a)

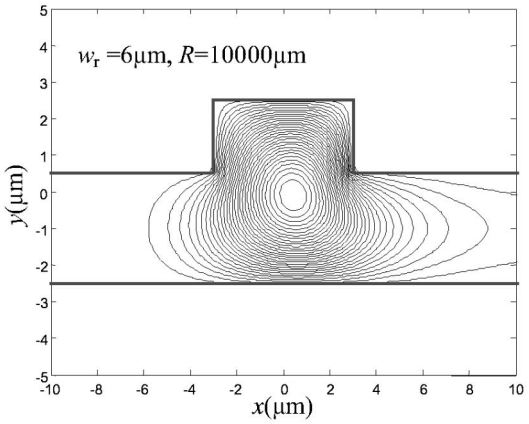

(b)

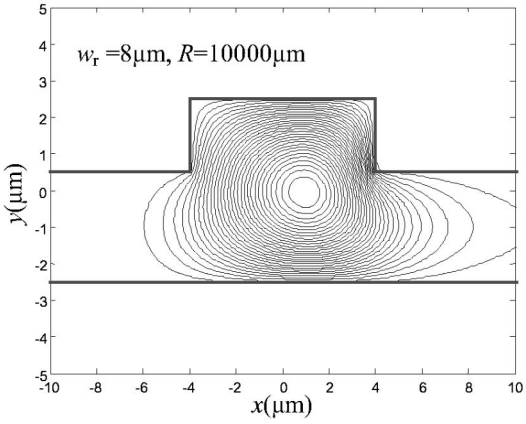

(c)

Fig. 6. Fundamental field profiles for bent waveguides with different rib widths when $R = 10{,}000\ \mu$m. (a) $w_r = 4\ \mu$m, (b) $w_r = 6\ \mu$m, (c) $w_r = 8\ \mu$m.

loss and the transition loss for the fundamental mode (E_{11}^x) and the higher-order modes (E_{21}^x and E_{12}^x) as the bending radius increases. Here the transition loss for a higher-order mode refers to the coupling loss from the fundamental mode of the straight waveguide to the higher-order mode of the bent waveguide.

From Figs. 7(a) and 7(b) one can see that the characteristics of the fundamental mode (here $h_r = 3.0\ \mu$m) are similar to those shown in Figs. 3(a) and 3(b) (where $h_r = 2.0\ \mu$m). However, the minimal bending radius (with an allowable pure bending loss of 0.1 dB/90°) is much smaller than that of the previous case when $h_r = 2.0\ \mu$m.

Figure 7(c) indicates that the pure bending loss of the E_{21}^x mode decreases as the bending radius increases, which is similar to the case of the fundamental mode. When the rib width increases, the pure bending loss for the E_{21}^x mode decreases (this is because the E_{21}^x mode is far from the cutoff). When $w_r = 4.0\ \mu$m, the pure bending loss for the E_{21}^x mode increases as the bending radius increases, which may look unreasonable. This is because the pure bending loss is given per 90° (instead of per centimeter) in Fig. 7(c). In fact, our calculation results have shown that the pure bending loss per centimeter decreases (as expected) when the bending radius increases.

The transition loss for the E_{21}^x mode is shown in Fig. 7(d), from which one can see that the transition loss decreases to a mininal value and then increases as the bending radius increases. This can be explained by analysis of the field distribution of the E_{21}^x mode. The modal field distorts significantly when the bending radius is very small. When the bending radius increases, the distortion is reduced, and the coupling efficiency between the fundamental mode of the straight waveguide and the E_{21}^x mode of the bent waveguide increases (i.e., the transition loss is reduced). However, when the bending radius increases further, the modal field of the bent waveguide becomes similar to that of a straight waveguide, and thus the E_{21}^x modal field approaches an odd symmetry. Since the fundamental mode of a straight waveguide has an even symmetry, the coupling efficiency (between the fundamental mode of the straight waveguide and the E_{21}^x mode of the bent waveguide) decreases when the bending radius increases further. When the bending radius approaches infinity, the transition loss for the E_{21}^x mode also approaches infinity.

From Fig. 7(d) one can also see that the transition loss for the E_{21}^x mode decreases when the rib width increases. For a bent waveguide, the peak of the modal field distribution (for both odd and even modes) deviates from the central axis of the waveguide. When the rib width increases, the symmetries of the modes are more distorted, and thus the coupling efficiency (between the fundamental mode of a straight waveguide and the E_{21}^x mode of a bent waveguide) increases (i.e., the transition loss decreases).

The pure bending loss and the transition loss for the E_{12}^x mode are shown in Figs. 7(e) and 7(f), respectively. From Fig. 7(f) one sees that the transition loss for the E_{12}^x mode increases as the bending radius increases [this is similar to the case of E_{21}^x shown in Fig. 7(d)]. The pure bending loss for the E_{12}^x mode is shown in Fig. 7(e), which is quite different from Fig. 7(c) for the E_{21}^x mode. From Fig. 7(e) one can see that the characteristics of the pure bending loss for the E_{12}^x mode differ very much for differ-

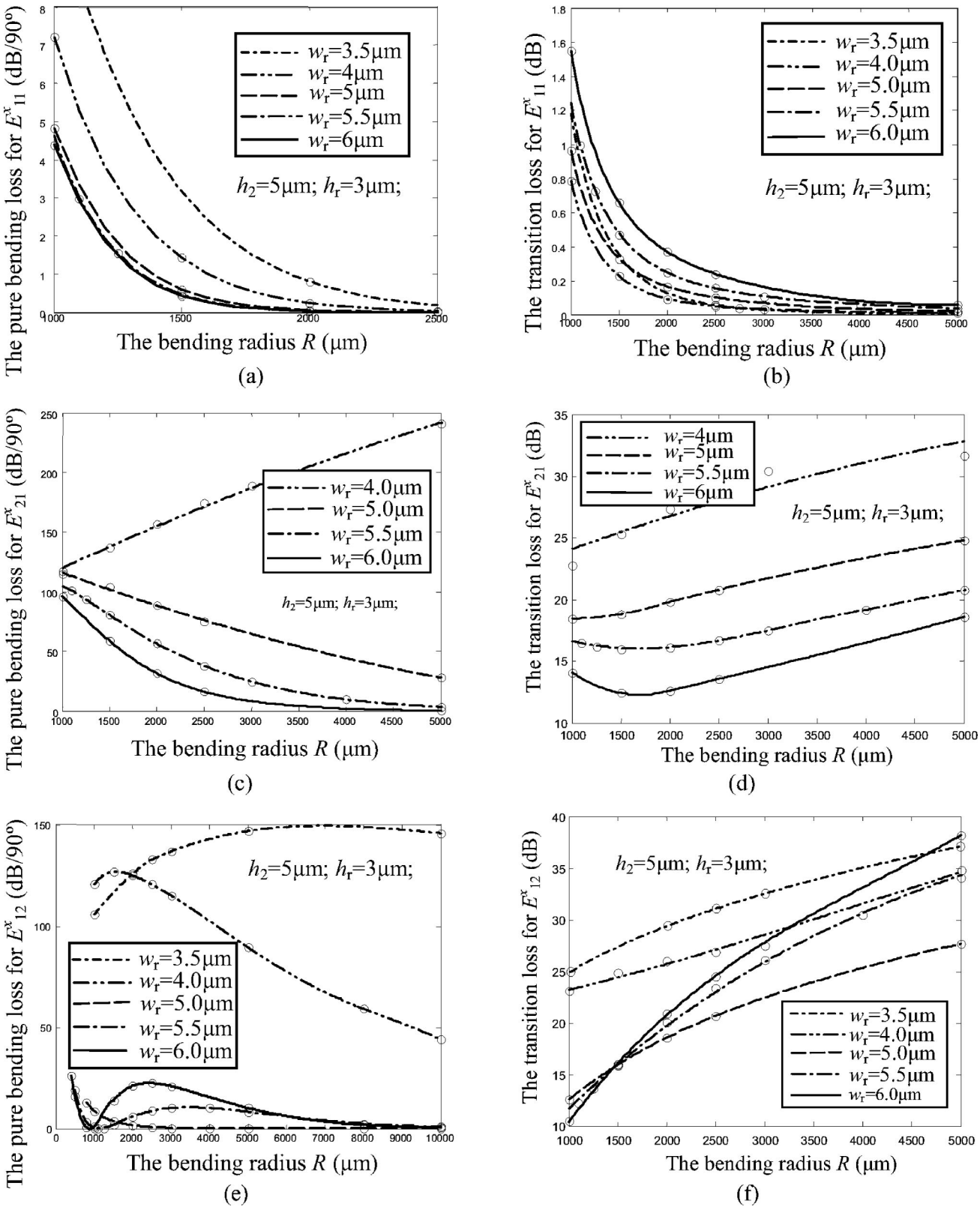

Fig. 7. Bending loss for the eigenmodes $E_{11}{}^x$, $E_{21}{}^x$, and $E_{12}{}^x$ of the bent waveguide when $h_r = 3.0\ \mu$m. (a) The pure bending loss for $E_{11}{}^x$, (b) the transition bending loss for $E_{11}{}^x$, (c) the pure bending loss for $E_{21}{}^x$, (d) the transition bending loss for $E_{21}{}^x$, (e) the pure bending loss for $E_{12}{}^x$, (f) the transition bending loss for $E_{12}{}^x$.

ent rib widths. For example, when $w_r = 4.0\ \mu$m the pure bending loss for the $E_{12}{}^x$ mode increases to a maximal value and then decreases as the bending radius increases. Like Fig. 7(c), the nonmonotonic behavior of Fig. 7(e) is due to the fact that the pure bending loss is given per 90° (instead of per centimeter). Our calculation has shown

that the pure bending loss per centimeter decreases monotonously (as expected) when the bending radius increases. For the case of $w_r = 5.0\ \mu$m, the pure bending loss for the E_{12}^x mode decreases as usual when the bending radius increases. When $w_r = 5.5$ and $6.0\ \mu$m, the curves of the pure bending loss are nonmonotonous in Fig. 7(e) for the E_{12}^x mode. The pure bending loss decreases to a minimal value, then increases to a maximal value, and then again decreases when the bending radius increases. This strange behavior can still be explained from analyzing the field distributions of the E_{12}^x modes shown by Figs. 8(a)–8(f) for bent waveguides with different radii (R = 10,000, 5000, 2000, 1000, 800, and 500 μm, respectively).

From these figures one can see that there are two peaks (referred to as the top peak and the bottom peak) in the vertical direction for the E_{12}^x mode. When the bending radius decreases from a very big value (close to infinity), both peaks shift outward, and the power leaking outward increases [see Figs. 8(a) and 8(b)]. The outward shift of the top peak is less than that of the bottom peak, since the top peak is more confined (by the rib). In this case the pure bending loss mainly results from the leakage loss of the bottom peak. When the bending radius decreases further, the top peak shifts outward further. However, the outward shift is prevented by the confinement of the rib. The outward shift of the top peak becomes a downward shift. The top peak is compressed in the lateral direction while being extended in the vertical direction [see Fig. 8(c)]. At the same time, the bottom peak is squeezed by the top peak, and thus the outward shift of the bottom peak is prevented by the top peak, which reduces the power leaking outward from the bottom peak. Thus the pure bending loss [dominated by the leakage from the bottom peak in this case; see Fig. 8(d)] of the bent waveguide is reduced. When the bending radius decreases further, the top peak shifts downward so much that it lies below the rib, and thus the power leaking outward from the top peak increases [see Figs. 8(e) and 8(f)]. Therefore the pure bending loss (dominated by the leakage from the top peak in this case) increases when the bending radius decreases further.

To remove the bad effects caused by the higher-order modes, one should ensure that the pure bending loss and the transition loss of the higher-order modes are large enough. A large transition loss means the power coupled from the fundamental mode to a higher-order mode is small. A large pure bending loss means the coupled power will attenuate rapidly along the propagation direction. Thus one should choose a small bending radius to make the pure bending loss of the higher-order modes large enough. On the other hand, Figs. 7(d) and 7(f) show that the bending radius should be chosen large enough to obtain a large transition loss. In addition, the low bending loss of the fundamental mode E_{11}^x also requires the bending radius to be large enough (typically, the pure bending loss and the transition loss are required be lower than 0.1 dB). Therefore geometrical parameters such as the rib height, the rib width, and the bending radius should be chosen appropriately. By optimizing the geometrical parameters of the bent waveguide, we can let only one mode (the fundamental mode) propagate with a low loss in a MM bent waveguide.

As a numerical example, we require the transition loss and the total bending loss for higher-order modes to be larger than 20 and 60 dB, respectively. We choose $h_r = 3.0\ \mu$m, and the other geometrical parameters can be determined from Figs. 7(a)–7(f) as follows:

1. The case of $w_r = 6\ \mu$m. According to the loss requirement for modes E_{11}^x, E_{12}^x, and E_{21}^x, the bending radius R should be larger than 4000, 2000, and 8000 μm, respectively. Thus we should choose $R \geqslant 8000\ \mu$m.
2. The case of $w_r = 5\ \mu$m. To satisfy the loss requirement for the modes of E_{11}^x, E_{12}^x, and E_{21}^x, we should let R be larger than 2500, 3000, and 2250 μm, respectively. Thus we choose $R \geqslant 3000\ \mu$m.
3. The case of $w_r = 4\ \mu$m. To satisfy the low-loss requirement for the fundamental mode (E_{11}^x), R should be larger than 2250 μm, for which the bending losses for E_{12}^x and E_{21}^x are large enough [see Figs. 7(c)–7(f)]. Thus we choose $R \geqslant 2250\ \mu$m.
4. The case of $w_r = 3.5\ \mu$m. To satisfy the low-loss requirement for the fundamental mode, R has to be larger than 2750 μm. The corresponding bending loss for E_{12}^x is large enough [see Figs. 7(e) and 7(f)]. Thus we choose $R > 2750\ \mu$m (the E_{21}^x mode does not exist in this case).

Therefore, for the same loss requirement in the above four cases, the bending radius is the smallest (2250 μm) when $w_r = 4\ \mu$m. From Fig. 5 one can also see that the optimal value for the rib width is approximately 4 μm when $h_r = 3.0\ \mu$m.

B. Design Procedure for a Bent Waveguide

Here we illustrate the design procedure with a specific example. Figure 9 shows the SOI rib waveguide structure to be designed, which is a part of an arrayed waveguide in an AWG demultiplexer. The arc is 60°. The optimal design for such a structure can be described as follows.

1. Determine the height and the width of the rib for the straight rib waveguide parts according to the SM condition and other requirements such as the coupling efficiency between the rib waveguide and a standard SM fiber. In this example, we have $h_r = 3\ \mu$m and $w_r = 3\ \mu$m for the straight rib waveguide parts.
2. To avoid any additional etching process, we ensure that the bent waveguide has the same rib height as the straight rib waveguide [determined in step (1)]. We then determine the optimal values for the rib width of the bent waveguide and the bending radius in the way given in the numerical example at the end of Subsection 3.A. The bending radius is determined according to the allowable loss for the fundamental mode and the minimal loss for the higher-order modes. In this numerical example, the optimal rib width of the MM bent waveguide is 4 μm, and the bending radius is determined to be 2250 μm.
3. Connect the two straight waveguides with the bent waveguide by use of two adiabatic tapered waveguides. The length of the taper section is 1200 μm.

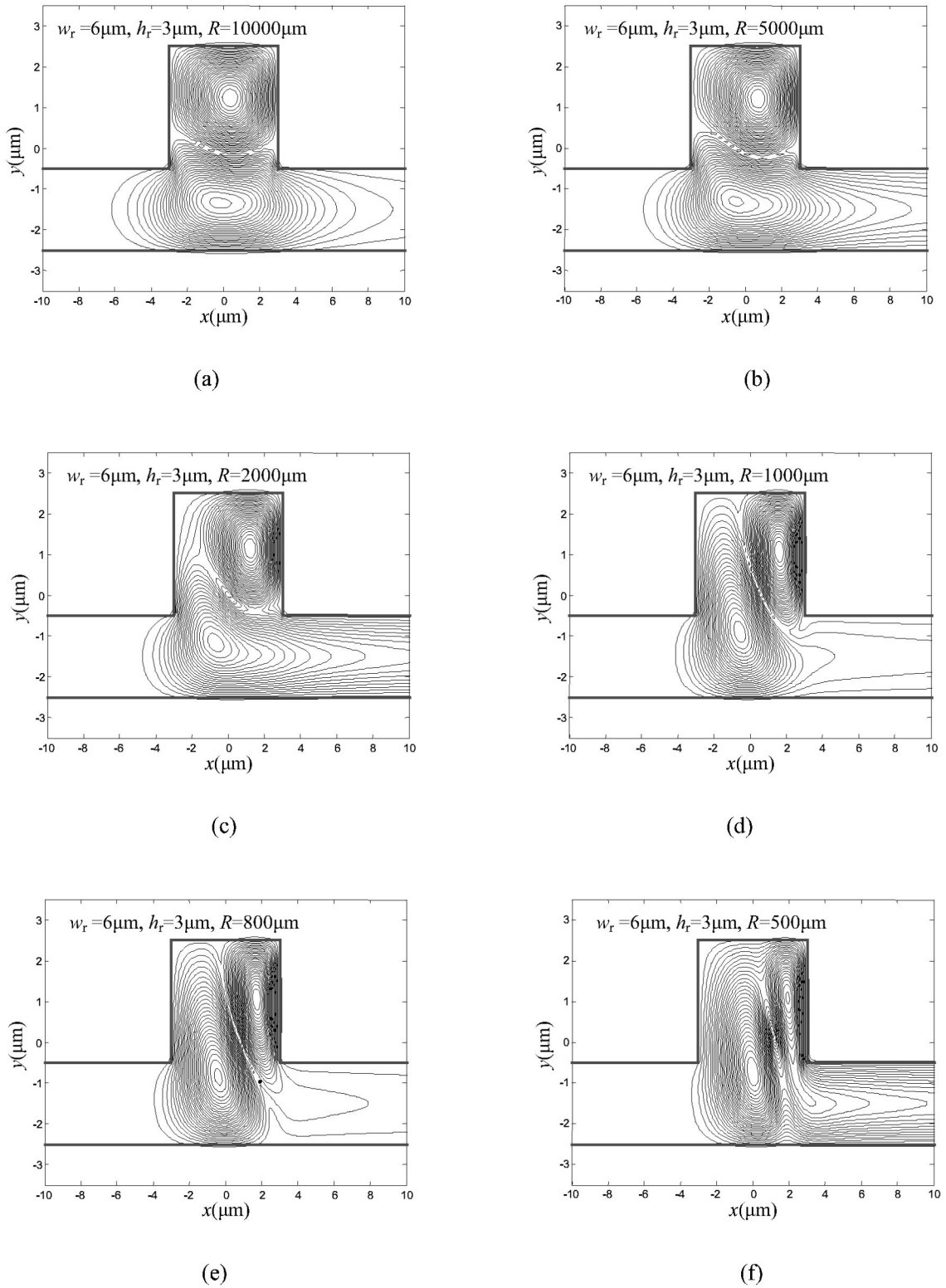

Fig. 8. Field distribution for the $E_{12}{}^{x}$ mode of a bent waveguide (w = 6.0 μm) with different radii. (a) R = 10,000 μm, (b) R = 5000 μm, (c) R = 2000 μm, (d) R = 1000 μm, (e) R = 800 μm, (f) R = 500 μm.

A three-dimensional finite-difference beam-propagation method[9,10] (with a perfectly matched layer boundary treatment) is used to simulate the light propagation in the structure. If the bent waveguide has the same rib width as the straight rib waveguide (i.e., 3 μm), the total propagation loss is approximately 1.41 dB. When we in crease the rib width of the bent waveguide to 4 μm (the optimally designed rib width), the total propagation loss

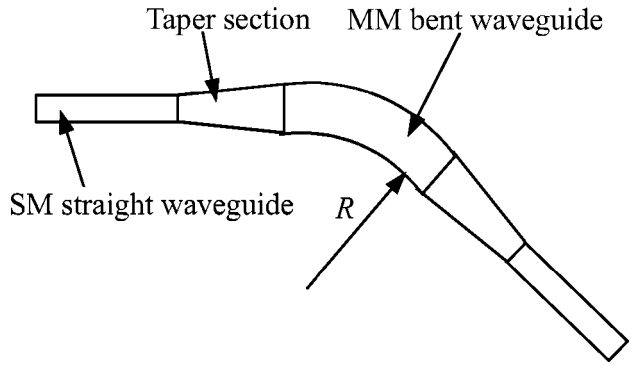

Fig. 9. Connecting a bent waveguide with two straight waveguides.

can be reduced to approximately 0.34 dB, which includes the loss in the two tapered sections (approximately 0.05 dB for each tapered section).

One can see that the bending loss of the fundamental mode in this structure is reduced significantly and the bad effects due to the higher-order modes are also reduced. Such a structure can be used to make the PIC more compact and thus improve the integration density.

4. CONCLUSION

The modal characteristics in a bent rib waveguide have been analyzed. The pure bending loss and the transition loss have been calculated and discussed. It has been shown that the bending radius can be reduced effectively by increase in the width and height of the rib. The undesired effects due to higher-order modes can be reduced when the bending losses of the higher-order modes are large enough. Thus a low-loss SM propagation in a MM bent waveguide can be realized. An arrayed waveguide in an AWG demultiplexer has been designed as a numerical example to illustrate the present design procedure. The numerical results given by the three-dimensional finite-difference beam-propagation method have shown that the bending loss for the fundamental mode of an appropriately designed MM bent waveguide can be much smaller than the bending loss for the fundamental mode of a SM bent waveguide with the same bending radius.

ACKNOWLEDGMENT

This research is supported by the Government of Zhejiang Province, China, under a major research grant (No.001101027).

Address correspondence to Daoxin Dai, Center for Optical and Electromagnetic Research, Department of Optical Engineering, Zhejiang University, Yu Quan, Hangzhou 310027, China. E-mail, dxdai@coer.zju.edu.cn.

REFERENCES

1. S. Kim and A. Gopinath, "Vector analysis of optical dielectric waveguide bends using finite-difference method," J. Lightwave Technol. **14**, 2085–2092 (1996).
2. M. L. Calvo and R. F. Alvarez-Estrada, "Three-dimensional analysis of bending losses in dielectric optical waveguides with arbitrary refractive-index profile," J. Opt. Soc. Am. A **4**, 683–693 (1987).
3. D. Dai, S. Liu, S. He, and Q. Zhou, "Optimal design of an MMI coupler for broadening the spectral response of an AWG demultiplexer," J. Lightwave Technol. **20**, 1957–1961 (2002).
4. N.-N. Feng, G.-R. Zhou, and W.-P. Huang, "Computation of full-vector modes for bending waveguide using cylindrical perfectly matched layers," J. Lightwave Technol. **20**, 1976–1980 (2002).
5. T. Yamamoto and M. Koshiba, "Numerical analysis of curvature loss in optical waveguides by the finite-element method," J. Lightwave Technol. **11**, 1579–1583 (1993).
6. J.-S. Gu, P.-A. Besse, and H. Melchior, "Method of lines for the analysis of the propagation characteristics of curved optical rib waveguides," IEEE J. Quantum Electron. **27**, 531–537 (1991).
7. S. P. Pogossian, L. Vescan, and A. Vonsovici, "The single-mode condition for semiconductor rib waveguides with large cross section," J. Lightwave Technol. **16**, 1851–1853 (1998).
8. M. K. Smit, E. C. M. Pennings, and H. Blok, "A normalized approach to the design of low-loss optical waveguide bends," J. Lightwave Technol. **11**, 1737–1742 (1993).
9. H. Deng, G. H. Jin, J. Harari, J. P. Vilcot, and D. Decoster, "Investigation of 3D semivectorial finite-difference beam propagation method for bent waveguides," J. Lightwave Technol. **16**, 915–922 (1998).
10. M. D. Feit and J. A. Fleck, Jr., "Analysis of rib waveguides and couplers by the propagating beam method," J. Opt. Soc. Am. A **7**, 73–79 (1990).